Emergent states in heavy-electron materials

Yi-feng Yang[a,1] and David Pines[b]

[a]Beijing National Laboratory for Condensed Matter Physics and Institute of Physics, Chinese Academy of Sciences, Beijing 100190, China; and
[b]Department of Physics, University of California, Davis, CA 95616

We obtain the conditions necessary for the emergence of various low-temperature ordered states (local-moment antiferromagnetism, unconventional superconductivity, quantum criticality, and Landau Fermi liquid behavior) in Kondo lattice materials by extending the two-fluid phenomenological theory of heavy-electron behavior to incorporate the concept of hybridization effectiveness. We use this expanded framework to present a new phase diagram and consistent physical explanation and quantitative description of measured emergent behaviors such as the pressure variation of the onset of local-moment antiferromagnetic ordering at T_N, the magnitude of the ordered moment, the growth of superconductivity within that ordered state, the location of a quantum critical point, and of a delocalization line in the pressure/temperature phase diagram at which local moments have disappeared and the heavy-electron Fermi surface has grown to its maximum size. We apply our model to CeRhIn$_5$ and a number of other heavy-electron materials and find good agreement with experiment.

heavy fermion | kondo liquid | spin liquid

Heavy-electron materials provide a unique f-electron laboratory for the study of the interplay between localized and itinerant behavior. At comparatively high temperatures, itinerancy emerges as the localized f-electrons collectively reduce their entropy by hybridizing with the conduction electrons to form a new state of matter, an itinerant heavy-electron Kondo liquid that displays scaling (non-Landau Fermi liquid) behavior (1–8). The emergent Kondo liquid coexists with the hybridized spin liquid that describes the lattice of local moments whose magnitude has been reduced by hybridization until one reaches the comparatively low temperatures at which unconventional superconductivity and hybridized local-moment antiferromagnetism compete to determine the ground state of the system over a wide regime of pressures. In practice, the phases often coexist, as experiments on the 115 [CeRhIn$_5$ (9–11) and CeCoIn$_5$ (12)] and 127 [CePt$_2$In$_7$ (13)] Kondo lattice materials demonstrate. A major challenge for the heavy-electron community has been finding a consistent framework and simple phenomenological description of their measured emergent behaviors that include the pressure variation of the onset of antiferromagnetic ordering at T_N, the growth of superconductivity within that ordered state, the onset of quantum critical behavior, and the growth of the heavy-electron Fermi surface.

Although progress has been made on developing a phenomenological theory of Kondo lattice materials (6), we do not yet possess a microscopic theory of the emergence of the Kondo liquid as a new quantum state of matter that displays universal behavior below a characteristic temperature (1–3, 5), T^*, or a satisfactory general framework for characterizing the conditions necessary for the emergence of the competing low-temperature ordered states, because experiments (4) have shown that the seminal phase diagram proposed by Doniach (14) does not apply to most materials. In this paper we introduce the concept of "hybridization effectiveness" as the organizing principle responsible for the emergence of low-temperature order and show it leads to a new phase diagram that provides a realistic explanation for the emergence of different low-temperature phases for Kondo lattice materials. The role of hybridization effectiveness in reducing the

entropy of the lattice of local moments present at high temperatures can be described quantitatively through the pressure dependence of a simple parameter present in the phenomenological two-fluid description (1–8) of heavy-electron materials whose magnitude can be determined from fits to experimental data. We show that our approach makes possible a consistent physical explanation and quantitative description of the low-temperature behaviors of a number of heavy-electron materials and predicts the presence of a delocalization line in the pressure/temperature phase diagram. It offers promise of serving as a standard model of heavy-electron emergent behaviors and providing the basis for the development of a microscopic theory that explains these.

Model

Hybridization Effectiveness. In the two-fluid description, the heavy-electron Kondo liquid emerges below a characteristic temperature, T^*, as a collective hybridization-induced instability of the spin liquid that describes the lattice of local moments coupled to background conduction electrons. T^* is determined by the effective Ruderman–Kittel–Kasuya–Yosida (RKKY) interaction between the nearest-neighbor local moments (4); the emergent scaling behavior of the Kondo liquid is characterized by the heavy-electron order parameter (3),

$$f_h(T) = f_0\left(1 - \frac{T}{T^*}\right)^{3/2}, \qquad \textbf{[1]}$$

which extends from T^* to a comparatively low temperature, T_0, at which ordering begins to set in (7). Over this temperature range it coexists with the "hybridized" quantum spin liquid, whose individual components (that still interact through the intersite RKKY coupling) possess a spectral weight that diminishes with lowering temperature as $f_l(T) = 1 - f_h(T)$.

The pressure-dependent parameter, f_0, in Eq. **1** provides a direct measure of the ultimate effectiveness of the underlying collective hybridization in reducing the magnitude of strength of each localized f-moment. Importantly, as may be seen in the schematic summary of our findings in Fig. 1, it constrains the nature of the ground state. As long as $f_0 < 1$, hybridization is always incomplete, so antiferromagnetic local-moment order becomes possible at a temperature reduced by hybridization: It takes place in the presence of itinerant heavy electrons that can become superconducting, so that over a wide range of pressures local-moment order coexists with superconductivity of magnetic origin. At $f_0 = 1$, the collective hybridization of local moments becomes complete at $T = 0$; hence, if superconductivity is suppressed by application of a strong enough magnetic field, one expects to find a quantum critical point, denoting a $T = 0$ transition between f-electron local order and a fully itinerant heavy-electron state. For $f_0 > 1$, the hybridization of local moments is complete and
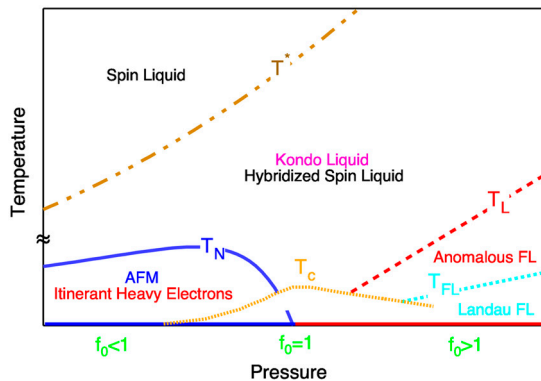
Fig. 1. A proposed phase diagram in which a quantum critical point at $f_0 = 1$ separates weak and strong hybridizing materials: If $f_0 < 1$, antiferromagnetic local-moment order in the presence of heavy electrons sets in below T_N; for $f_0 > 1$, one has complete delocalization of f-electrons along a line T_L, with the heavy electrons forming a Landau Fermi liquid below T_{FL}. Around the quantum critical point at $f_0 = 1$, the heavy electrons may condense into superconductivity below T_c because of magnetic quantum fluctuations. T^* marks the onset of Kondo liquid emergence produced by collective hybridization.

the Fermi surface will have grown to its maximum size at some finite temperature, T_L; Kondo liquid scaling behavior is expected between T^* and T_L, whereas T_L is fixed by f_0 and T^*. From Eq. **1**, we have:

$$\frac{T_L}{T^*} = 1 - f_0^{-2/3}. \qquad [2]$$

For f_0 close to 1, because of the proximity of a quantum critical point, immediately below T_L one does not expect to find Landau Fermi liquid (FL) behavior; instead, the properties of the heavy electrons will be determined by their coupling to quantum critical fluctuations; anomalous behavior, including further mass enhancement, continues until one reaches the still lower characteristic temperature, T_{FL}, shown in Fig. 1, at which transport and other properties are no longer dominated by the coupling of quasiparticles to quantum critical fluctuations, and one finds Landau Fermi liquid behavior.

The Hybridized Quantum Spin Liquid. The magnetic properties of the hybridized spin liquid can be studied by assuming its dynamic spin susceptibility takes a mean-field form,

$$\chi_l(q, \omega) = \frac{f_l \chi_0}{1 - z J_q f_l \chi_0 - i\omega/\gamma_l}, \qquad [3]$$

where χ_0 is the local susceptibility of an individual f-moment, z is the coordination number, γ_l is the local relaxation rate, and J_q is the RKKY exchange coupling. For simplicity, the magnetic moment of the f-spins and the Boltzmann constant are set to unity. The hybridized spin liquid will begin to order at a Néel temperature that is, according to Eq. **3**, determined by:

$$z J_Q f_l(T_N) \chi_0(T_N) = 1. \qquad [4]$$

All local physics can be included in the local-moment static susceptibility χ_0. For example, crystal field effects become important when the crystal field splitting from the ground-state doublet is smaller than or comparable to T^*; if the crystal field configuration is known and plays a role, it can be easily taken into account in χ_0. In this paper, we take for simplicity $\chi_0 = C/T$, where C is the Curie constant. For $T > T^*$, Eq. **3** reduces to the Curie–Weiss form of the static susceptibility, $\chi_l(0, 0) = C/(T + \theta)$, where $\theta = CzJ_{q=0}$. We have then

$$\frac{T_N}{T^*} = \eta f_l(T_N), \qquad [5]$$

where the parameter $\eta = CzJ_Q/T^*$ reflects the effect of the crystal lattice and magnetic frustration on T_N, whereas $f_l(T_N)$ reflects the role played by collective hybridization in reducing the Néel temperature. Because of the RKKY nature of both T^* and J_Q (4), η is pressure-independent.

The magnitude of the ordered moment μ^2 is determined by the local-moment order parameter:

$$\frac{\mu^2}{\mu_0^2} = f_l(T_N), \qquad [6]$$

where μ_0 is the local-moment strength above T^*. Where accurate measurements of the strength of the ordered moment in the antiferromagnetic state exist, a good test of our model is to combine Eqs. **5** and **6** to obtain an expression that relates three experimentally measurable quantities at a fixed value of η,

$$\frac{T_N}{T^*} = \eta \frac{\mu^2}{\mu_0^2}. \qquad [7]$$

Because T^* increases with increasing pressure, whereas μ decreases, it follows that in general the T_N versus pressure curve should exhibit the maximum shown in Fig. 1.

In applying Eqs. **5** and **6** to experiment, one needs to take relocalization effects into account. As discussed in apRoberts-Warren et al. (7) and Shirer et al. (8), Knight shift experiments demonstrate that Kondo liquid scaling ends at a temperature T_0, below which local-moment ordering begins to win out over collective hybridization in determining the temperature evolution of $f_l(T)$. As the temperature is lowered, the rate of collective hybridization is first reduced and then reversed—i.e., the spectral weight of $f_l(T)$ begins to increase as the temperature is further lowered. For the two materials for which this relocalization has been explored in detail, it turns out that $f_l(T_N)$ is approximately $f_l(T_0)$ and T_0 is approximately $2T_N$.

Determining f_0. We can use Eq. **3** to determine f_0 from measurements of the static spin susceptibility if we make the physically reasonable assumption that the hybridized spin liquid contribution is dominant for a broad range of temperatures below T^*. Such approximation is reasonable because of the large magnetic response of the local moments seen at temperatures above T^*. Fig. 2 shows the evolution of $\chi_l(0, 0)$ with f_0 and the fit to experimental data in several compounds—from the antiferromagnet
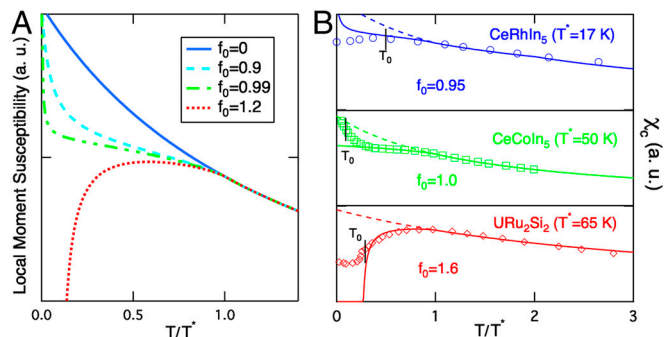
Fig. 2. The role played by hybridization effectiveness in determining the static magnetic susceptibility. (*A*) Schematic illustration of the influence of f_0 on $\chi_l(0, 0)$ for a fixed value of $\theta/T^* = 1.4$. (*B*) A comparison of our calculated and experimental values of the *c*-axis susceptibility χ_c for three materials: CeRhIn$_5$ (15), CeCoIn$_5$ (16), and URu$_2$Si$_2$ (17). The solid lines are theoretical fits with $\theta/T^* = 1.4, 1.35$, and 3.5, respectively; also shown is the temperature, T_0, at which scaling behavior is altered by the onset of low-temperature order.

CeRhIn$_5$ (15) to the superconductor CeCoIn$_5$ (16) to the 5f compound URu$_2$Si$_2$ that exhibits hidden order (17). We find $f_0 =$ 0.95 for CeRhIn$_5$, 1.0 for CeCoIn$_5$, and 1.6 for URu$_2$Si$_2$. With increasing f_0, we find a crossover from peak to plateau to peak structure in the uniform susceptibility of exactly the kind that has been observed in many heavy-electron materials. However, the origin of the peak seen in materials with $f_0 < 1$, such as CeRhIn$_5$, and those in which $f_0 > 1$, such as URu$_2$Si$_2$, is different. For $f_0 > 1$, the peak comes from rapid delocalization of the f-moments at approximately T^*; for $f_0 < 1$, it is related to the onset of relocalization of the Kondo liquid as a precursor of the antiferromagnetic ordering at $T_0 \ll T^*$ (7, 8).

The Kondo Liquid. The Kondo liquid contributes to the magnetic entropy and other material properties that display anomalous behavior, as well as physical quantities, such as transport and superconductivity, that originate uniquely in the itinerant f-electrons. The Kondo liquid entropy S_h can be obtained by integrating over the universal scaling expression for its specific heat $C/T \propto [1 + \ln(T^*/T)]$ (3) and recognizing that continuity at T^* requires that $S_h(T^*) = S_l(T^*) = R\ln 2$ (R is the gas constant). When the scaling behavior of the Kondo liquid ends at a temperature T_x ($=T_L$ if $f_0 > 1$), the two-fluid model predicts that the heavy-electron entropy will be given by (6):

$$S_h(T_x) = R\ln 2 \frac{T_x}{2T^*}\left[2 + \ln\left(\frac{T^*}{T_x}\right)\right]. \quad \text{[8]}$$

Below T_L, no local moments are present; only heavy electrons are responsible for the measured system behavior and a one-fluid picture is recovered, as may be verified in Knight shift measurement. The Fermi liquid-specific heat coefficient, γ_h, at lower temperatures can then be estimated:

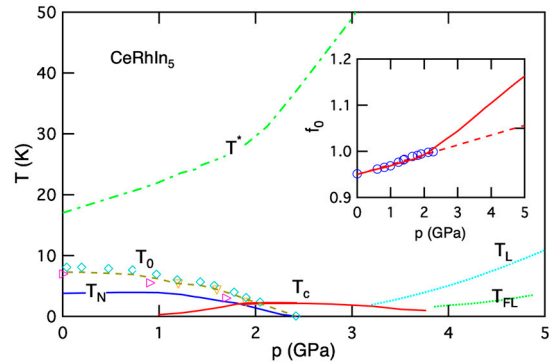$$\gamma_h \sim \frac{S_h(T_L)}{T_L} = \frac{R\ln 2}{2T^*}\left[2 - \ln\left(1 - f_0^{-2/3}\right)\right]. \quad \text{[9]}$$

In general, even when $f_0 < 1$ or $T > T_L$, the specific heat coefficient can still be calculated using Eq. **11**.

Results

Application to CeRhIn$_5$. CeRhIn$_5$ provides an excellent proving ground for the approach we have described. Our proposed phase diagram for CeRhIn$_5$ is given in Fig. 3, and resembles closely the experimental pressure/temperature phase diagram derived from the resistivity exponent (18). The Knight shift experiments of Shirer et al. (8) show that $f_l(T_N) \approx f_l(2T_N)$ at ambient pressure; we assume this to be true in the entire pressure range in the following analysis, with $f_l(2T_N)$ given by the scaling formula in Eq. **1**.

Antiferromagnetism. On applying Eqs. **5**, **6**, and **7** to CeRhIn$_5$, we obtain the results for the variation of the Néel temperature with pressure, and of the magnitude of the ordered moment found in the Néel state that is given in Fig. 4. Despite its simplicity, our model yields results in good agreement with experiment (19–24). Fig. 4A compares the experimental data of T_N and $\eta T^* f_l(2T_N)$. The best fit to the Néel temperature yields $\eta = 0.36$ for $f_0 = 0.95$. On taking the strength of the local moments above T^* to be 0.92 μ_B (25), $\eta = 0.36$ gives the right magnitude of the ordered moment when Eq. **7** is used together with the pressure variation of T_N. A corresponding best fit to the results of Aso et al. (23) and Llobet et al. (24) requires that $\eta = 0.64$ and 0.32, respectively. Our results are seen to be more consistent with those of Llobet et al. (24).
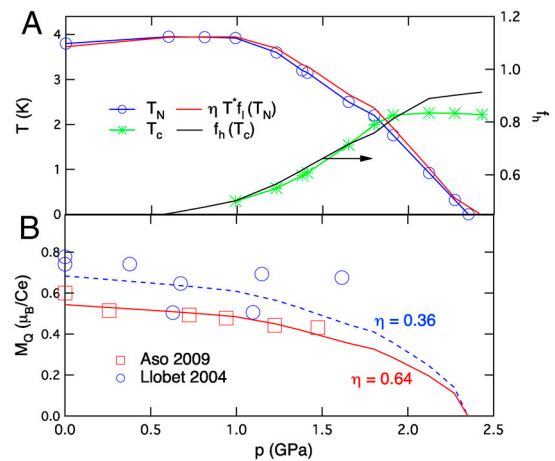
In our mean-field approach, the influence of the crystalline lattice and magnetic frustration are incorporated in the coordination number z and $\eta = CzJ_Q/T^*$. To illustrate a reasonable range for these parameters, we consider a 2D square lattice for which the RKKY coupling has the usual form $J_q = J_n[\cos(q_x) + \cos(q_y)] + 2J_{nn}\cos(q_x)\cos(q_y)$, where J_n and J_{nn} are the nearest- and next-nearest neighbor couplings, respectively. We have $\theta = 2Cz|J_n + J_{nn}|$ and $\eta T^* = 2Cz|J_n - J_{nn}|$ for $Q = (\pi, \pi)$. If we take the values $\eta = 0.36$ and $\theta/T^* = 1.4$, obtained in the susceptibility fit in Fig. 2B, we find a frustration ratio $J_{nn}/J_n \approx 0.6$. This indicates $T^*/2Cz|J_n|$ of approximately 1.1, consistent with its origin in nearest-neighbor RKKY coupling (4).

Itinerant Electrons and Superconductivity Within the Néel State. Our model provides a natural explanation for the appearance of superconductivity within the Néel state and the pressure depen-

Fig. 3. The proposed phase diagram of CeRhIn$_5$. The pressure dependence of T_N and T_c are taken from refs. 18 and 19, whereas the coherence temperature T^* is that determined by Yang et al. (3, 4, 6). The experimental points determining T_0, the cutoff temperature for Kondo liquid scaling, reflect its signature in several different experimental probes: a pseudo–gap-like feature in the spin-lattice relaxation rate (20), a change in the anomalous Hall effect (21) and inelastic neutron-scattering spectrum (22), and a peak in the measured "anomalous" Kondo liquid susceptibility (15). T_L is the delocalization temperature expected if $f_0(p)$ is approximately $J\rho$, where J is the local Kondo coupling and ρ is the density of states of the conduction electrons. (*Inset*) The hybridization parameter $f_0(p)$ as a function of pressure: The points are derived from $T_N(p)$; the solid line is its behavior at higher pressures if f_0 scales with the Kondo coupling, $J\rho$, in the vicinity of the quantum critical point; and the dashed line is a simple linear extrapolation.

Fig. 4. The Néel temperature, superconducting transition temperature, and ordered moments as a function of pressure in CeRhIn$_5$. (*A*) Comparison between experimental $T_N(p)$ (18, 19) and $\eta T^* f_l(T_N)$, and between $T_c(p)$ and $f_h(T_c)$ derived from $f_0(p)$ in Fig. 3, *Inset*, for CeRhIn$_5$. With $f_0 = 0.95$, the best fit requires $\eta = 0.36$ in the presence of relocalization. (*B*) The pressure evolution of the Ce-staggered moment at $Q = (\pi, \pi)$. Open squares are data reported by Aso et al. (23) and open circles are reproduced from Llobet et al. (24). The dashed line is our theoretical result with $\eta = 0.36$ and the solid line is the fit for Aso's data with $\eta = 0.64$. For Llobet's data, the best fit requires $\eta = 0.32$.

dence of its transition temperature, T_c. Quite generally, local-moment ordering takes place before the relocalization process is complete. Below T_N, a substantial number of heavy electrons coexist with the ordered local moments in the antiferromagnetic phase, a fraction that increases as the pressure increases. For example, in CeRhIn$_5$, despite relocalization, $f_h(T_N)$ is approximately 0.37 at ambient pressure. How do these heavy electrons lose their entropy within the Néel state? There are two possibilities: (*i*) The relocalization process continues within the Néel state; or (*ii*) the heavy-electrons order, most likely in an unconventional superconducting state because there are ample magnetic fluctuations present that can bring this about (26). Both likely occur in practice.

Where superconductivity emerges, it is appealing to argue that, to a first approximation, T_c scales with the density of heavy electrons present, an argument familiar from the well-known Uemura plot for the cuprate superconductors (27). We test this hypothesis by comparing the growth in T_c with pressure with the corresponding growth in the density of heavy electrons. As may be seen in Fig. 4*A*, the increase in T_c seen from 1 GPa to 1.75 GPa mirrors the increase in the density of heavy electrons able to participate in superconductivity, $f_h(T_c) = f_h(2T_N)$ assuming no further relocalization below T_N. Further confirmation of this view of Kondo liquid behavior comes from the scaling of the Knight shift anomaly above and below T_c seen in CeCoIn$_5$ (5), and the observation that T_c is maximum in the vicinity of the critical pressure at which some part of the heavy-electron Fermi surface can begin to localize.

Fermi Liquid Regime. At pressures $p > 2.35$ GPa, the hybridization parameter is $f_0 > 1$, so the ground state of CeRhIn$_5$ should be a Fermi liquid if one applies a magnetic field strong enough to suppress superconductivity. At $T_L = (1 - f_0^{-2/3})T^*$, when hybridization is complete, our model predicts a heavy electron-specific heat that depends only on T^* and f_0 and is given by Eq. 9. T_L can be determined from a measurement of the Fermi surface, which should reach its maximum size there. Our analysis at low pressures suggests that f_0 may scale with the Kondo coupling, J, in the vicinity of the quantum critical point. If this scaling extends to higher pressures, it leads to the results shown for T_L in Fig. 3. Below T_L, the f-electrons form a Fermi liquid, but its quasiparticles, being scattered by quantum critical spin fluctuations, do not exhibit the classic properties proposed by Landau until one reaches a lower-temperature T_{FL}.

Spin-Lattice Relaxation Rate. Nuclear magnetic/quadrupole resonance (NMR/NQR) experiments on the pressure dependence of the spin-lattice relaxation rate provide a further confirmation of the approach developed here. We assume that the spin-lattice relaxation rate between T^* and T_0 is dominated by local-moment behavior and calculate it using the Moriya formula (28),

$$\frac{1}{T_1} = \gamma^2 T \lim_{\omega \to 0} \sum_q F(q)^2 \frac{\mathrm{Im}\chi_l(q,\omega)}{\omega}, \qquad [10]$$

where γ is the gyromagnetic ratio and $F(\mathbf{q})^2$ is the form factor. Following ref. 29, we use $F(\mathbf{q})^2 = F_0^2[\cos(\mathbf{q}_x/2)^2 \cos(\mathbf{q}_y/2)^2 + x^2 \sin(\mathbf{q}_x/2)^2 \sin(\mathbf{q}_y/2)^2]$, where x, the only free parameter, defines the anisotropy of the hyperfine coupling. On using the values of $f_0(p)$ given in Fig. 3 (*Inset*) and assuming that J_q is close to its value for a 2D square lattice, we obtain the fit to the NQR data in CeRhIn$_5$ shown in Fig. 5. We see there the expected change in slope caused by hybridization for T_1^{-1} and that our model provides a fit to experiment above T_0, with $T^* = 17$ K at 0 GPa, 20 K at 0.46 GPa, and 25 K at 1.23 GPa, respectively, and an anisotropy parameter x at ambient pressure of 0.08 that increases to 0.12 at 0.46 GPa and 0.2 at 1.23 GPa, in agreement
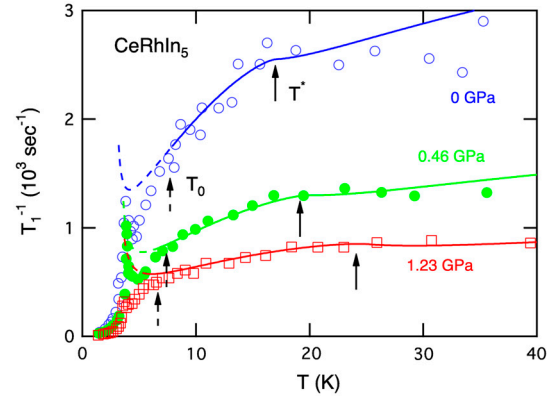
Fig. 5. Comparison of measured and calculated NQR spin-lattice relaxation rate at ambient pressure, 0.46 GPa and 1.23 GPa, in CeRhIn$_5$ (20). The solid lines are our theoretical fit with $T^* = 17$ K, 19 K, and 24 K, and $x = 0.08$, 0.12, and 0.2, respectively.

with earlier estimates (29). The behavior found above T^* reflects the comparatively weak local-moment interaction; the temperature dependence seen between T_0 and T_N originates from the precursor antiferromagnetic fluctuations (22) and Kondo liquid relocalization (7), and cannot be calculated using the present mean-field approximation. The local relaxation rate γ_l has been assumed to be a constant in the fit; a temperature-dependent γ_l may yield improved agreement between theory and experiment.

Magnetic Entropy. The magnetic entropy is another important quantity of experimental interest. In many heavy-electron antiferromagnets, one finds a small entropy release at T_N despite the presence of large ordered moment. As will be shown below, our expanded two-fluid model explains these apparently contradictory results as a direct consequence of hybridization and yields agreement with experiment for the magnetic entropy of a number of heavy-electron materials.

Above T^*, the magnetic entropy is that of localized f-electron moments in a ground-state doublet that is assumed to have the full magnetic entropy $R \ln 2$. At lower temperatures, both the local moments and the Kondo liquid contribute and the total magnetic entropy is given by ref. 6 as:

$$S(T) = R \ln 2 \left[f_l(T) + f_h(T) \frac{T}{2T^*} \left(2 + \ln \frac{T^*}{T} \right) \right]. \qquad [11]$$

We expect Eq. 11 to be valid down to a temperature T_0, at which low-temperature order begins to compete with hybridization in reducing the local-moment entropy. Above T_0 and for arbitrary f_0, where Eq. 9 does not apply, the specific heat coefficient can still be estimated from the temperature derivative of Eq. 11. For CeRhIn$_5$, as shown in Fig. 3, a number of different experimental probes suggest that T_0 is of order of $2T_N$; importantly, the measurements by Shirer et al. of the Knight shift anomaly show that Kondo liquid behavior is strongly suppressed below T_0, indicating a rapid relocalization of itinerant heavy electrons (7, 8).

The physics below T_0 require that Eq. 11 be modified. In addition to a deviation from scaling in the order parameters f_h and f_l, the contribution of each component to the magnetic entropy is expected to be reduced from its value at T_0 by the approach of antiferromagnetic order. On comparing the magnetic entropy calculated from Eq. 11 with experiment for CeRhIn$_5$ (19), we find that a factor of r_N of approximately 0.35 has to be introduced at ambient pressure in order to obtain agreement with experiment; a reduction of this size is justified by the similar ratio $S(T_N)/S(T_0)$ of approximately 0.4 found in experiment (19). As may be seen in Fig. 6, with this factor one obtains good agreement with experiment for pressures up to 1.75 GPa. In contrast, at higher
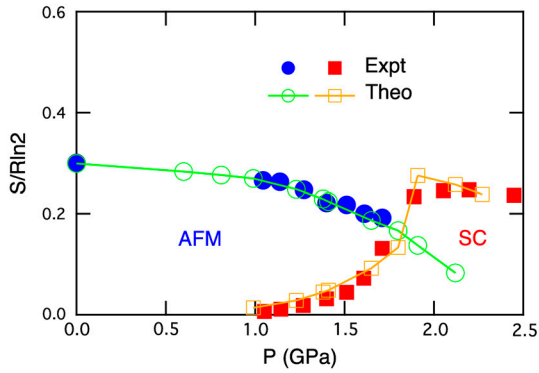
Fig. 6. Comparison of measured (19) and calculated magnetic entropies at the Néel temperature, T_N, and superconducting transition temperature, T_c, in CeRhIn$_5$ as a function of pressure (15, 19). Theoretical predictions are obtained by using $f_0(p)$ in Fig. 3, *Inset*.

pressures, where superconductivity takes over and the Kondo liquid scaling persists down to T_c, no corrections are needed to Eq. **11**, which yields good agreement with experiment for the entropy at T_c.

In calculating the entropy at the superconducting transition deep within the antiferromagnetic phase ($1.0 < p < 1.75$ GPa) shown in Fig. 6, we have excluded the contribution from the ordered moments, whose fraction, $a(T_c) = (1 - T_c/T_N)^{0.5}$, has been measured (24), and have assumed the Kondo liquid-specific heat does not change between T_N and T_c. The entropy release of the coexisting state is then given by

$$S(T_c) = r_N f_l(T_N)[1 - a(T_c)]R\ln 2 + r_N f_h(T_N)S_h(T_N)\frac{T_c}{T_N},$$

[12]

and agrees well with experiment.

At first sight, given the comparatively large magnitude of the ordered moment in CeRhIn$_5$ (0.6–0.8 μ_B), the entropy released by the antiferromagnetic ordering of the local moments appears unexpectedly small, being only approximately 30% $R\ln 2$ (15). A little thought shows that the reduction comes in three sequential stages, corresponding to the entropy release at T_N, T_0, and T^*, respectively. When antiferromagnetism is destroyed at $T_N = 3.8$ K, only a fraction (approximately 63%) of the spectral weight of the strongly hybridized f-moments is available to become "free"; the rest (approximately 37%) of that spectral weight has already gone to the Kondo liquid, whose entropy is already much reduced because of strong entanglement between conduction and f-electrons. It follows that above T_N, the entropy of the freed moments is then only released at a higher temperature T_0 of approximately 8 K because of strong magnetic correlations close to the phase transition (8), whereas the total spin entropy will not be fully recovered until all the correlated Kondo liquid has been transformed into uncorrelated f-moments above $T^* = 17$ K. The continuous and slight change of the magnetic entropy at the ordering temperature as one moves from antiferromagnetism to superconductivity with increasing pressure range requires a gradual change of character of f-moments and argues against a dramatic change of hybridization across the quantum critical region.

Application to Other Materials. In applying our model to other prototypical heavy-electron materials, we focus on the relation between f_0 and the magnetic/nonmagnetic ground state, and the entropy release of the ordered state (when $f_0 < 1$) or the residual specific heat coefficient of the Fermi liquid (if $f_0 > 1$), because these only require experimental input at ambient pressure. Our results are summarized in Fig. 7 and Table 1, and discussed in the
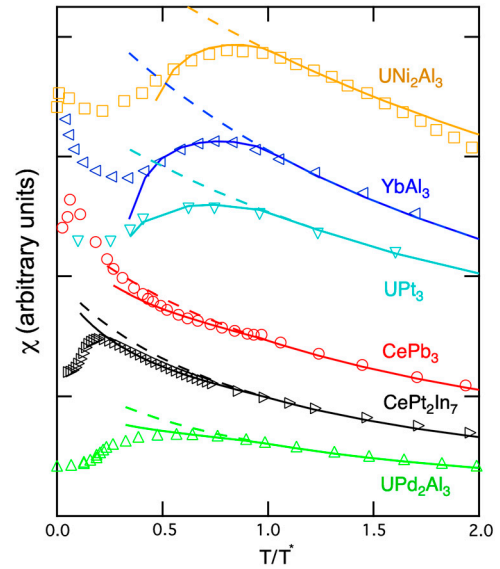
Fig. 7. Magnetic susceptibility of several prototypical heavy-electron materials. The solid lines are our theoretical fit using the mean-field formula and the dashed lines are the Curie–Weiss susceptibility. The fitting parameters are shown in the text.

subsections below. Because they are strong hybridizers ($f_0 > 1$), we conclude that UNi$_2$Al$_3$ must be a spin-density wave antiferromagnet in which antiferromagnetic order originates from Fermi surface nesting of the heavy-electron Kondo liquid (30), whereas the hidden-order transition in URu$_2$Si$_2$ must be caused by a Kondo liquid instability (31). As may be seen in Fig. 8, our model [Eq. **9**] also yields results for the low-temperature Fermi liquid-specific heat of a number of materials that are surprisingly close to their experimental values (17, 32–35), which demonstrates that, for these materials, the average heavy-electron effective mass is determined by the onset of collective hybridization at T^* and its effectiveness, f_0.

CeCoIn$_5$. For this material, the Kondo liquid temperature $T^* = 50$ K has been determined using a number of experimental probes (3, 4). On using Eq. **3**, we show in Fig. 2B that f_0 of approximately 1 provides a good fit to the susceptibility data (16, 35), a conclusion that is consistent with the expectation that CeCoIn$_5$ is close to a magnetic quantum critical point (36). We find $S(T_c) = 0.18\,R\ln 2$, close to the experimental value of 0.2 $R\ln 2$ at $T_c = 2.3$ K (35). Taking T_c as the cutoff temperature, the predicted specific heat coefficient at T_c and zero field using Eq. **11** is approximately 368 mJ/mol K^2, comparable to the experimental value of approximately 290 mJ/mol K^2 (17).

Table 1. Hybridization effectiveness and low-temperature order

Materials	T^* (K)	$T_{N/L/c}$ (K)	f_0	Order
Local-moment order				
CePt$_2$In$_7$	41	5.6	0.4	AFM
CePb$_3$	16	1.1	0.5	AFM
UPd$_2$Al$_3$	60	14.3	0.8	AFM
CeRhIn$_5$	17	3.8	0.95	AFM
Kondo liquid order				
CeCoIn$_5$	50	2.3	1.0	SC
UPt$_3$	25	5	1.4	SC
YbAl$_3$	160	38	1.5	FL
URu$_2$Si$_2$	65	17.5	1.6	HO
UNi$_2$Al$_3$	120	39	1.8	SDW

AFM, antiferromagnetism; SC, superconductivity; FL, Fermi liquid; HO, hidden order; SDW, spin-density wave antiferromagnetism.
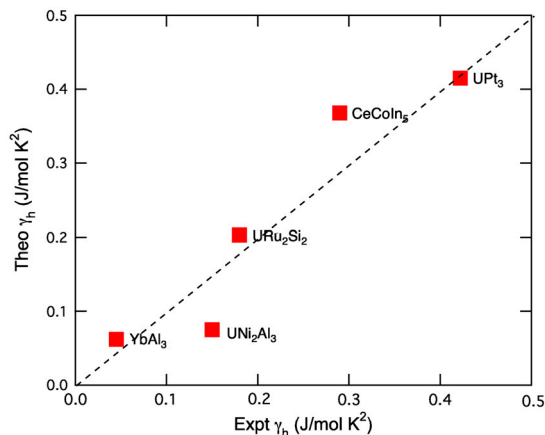
Fig. 8. A comparison between the values of the specific heat coefficient predicted by our model and experiment for materials with $f_0 \geq 1$ (17, 32–35).

URu$_2$Si$_2$. As may be seen in Fig. 2B, our best fit to the c-axis susceptibility of URu$_2$Si$_2$ gives the hybridization parameter $f_0 = 1.6$, and T_L of approximately T_{HO}. Below T_L, all f-electrons become itinerant so that a single-component picture is recovered and the Knight shift becomes once again proportional to the susceptibility. This allows us to subtract the spin susceptibility of the two components without uncertainty, and the detailed analysis given in ref. 8 yields similar results for f_0 and T_L. These suggest that most local moments have disappeared by the time one reaches T_{HO}, so that the hidden-order transition must have an itinerant and strongly correlated nature, consistent with experimental observation of gap opening (37, 38) and Fermi surface reconstruction at T_{HO} (39). Our predicted entropy release at T_{HO} is 0.44 $R \ln 2$, somewhat larger than the experimental value of 0.3 mJ/mol K^2 (17). The predicted specific heat coefficient without hidden order is approximately 203 mJ/mol K^2, close to the experimental extrapolated value of 180 mJ/mol K^2.

CePt$_2$In$_7$. Using $\theta = T^* = 41$ K, we find $f_0 = 0.4$ from a fit to the susceptibility, in which only the local-moment contribution is included. In an earlier analysis that included the Kondo liquid contribution and assumed a Wilson ratio $R_W = 2$ (7), f_0 was found to be approximately 1, a result in obvious contradiction with the magnetic ground state. The contradiction leads us to conclude that one should not in general assume that $R_W = 2$, but, rather, determine it on a case-by-case basis. For this material, NMR measurements point to a relocalization temperature T_0 of approximately 14 K, below which the magnetic entropy is strongly suppressed. Our scaling result yields $S(T_N) = 0.76 \, R \ln 2$, which is very much larger than the experimental value of approximately 0.2 $R \ln 2$ (12): Just as was the case with CeRhIn$_5$, relocalization effect is large between $T_0 = 14$ K and $T_N = 5.6$ K, a result that is consistent with the NMR experimental results (7).

CePb$_3$. The susceptibility of CePb$_3$ has a plateau below $T^* = 16$ K, followed by a peak before the magnetic transition at $T_N = 1.1$ K (40). Our best fit gives $f_0 = 0.5$ and $\theta = 25$ K, and yields an entropy release of approximately 0.62 $R \ln 2$ at T_N, which is large compared to the experimental value of 0.32 $R \ln 2$, a discrepancy that is likely caused by the rapid suppression of the magnetic entropy between approximately 3 K and T_N (see figure 8 in ref. 40).

UPt$_3$. Our fit to the susceptibility of UPt$_3$ gives $f_0 = 1.4$, $\theta = 71$ K, and $T^* = 25$ K. We find T_L of approximately 5 K, consistent with the deviation from scaling seen in the Knight shift anomaly

(3), and $\gamma_h = 415$ mJ/mol K^2, in good agreement with the experimental value of 422 mJ/mol K^2 (33).

UM$_2$Al$_3$. UPd$_2$Al$_3$ and UNi$_2$Al$_3$ are both antiferromagnetic at low temperatures but, as our fit to the susceptibility shows, their physical origins are different. Because of crystal field effects, for UPd$_2$Al$_3$ (4, 41) we can only give a rough estimate of $\theta = T^* = 60$ K and $f_0 = 0.8$, whereas for UNi$_2$Al$_3$ (34) we find $T^* = 120$ K, $\theta = 420$ K, and $f_0 = 1.8$. These quite different values of f_0 strongly suggest that the magnetic ground state of UPd$_2$Al$_3$ originates in ordering of its local moments, whereas that of UNi$_2$Al$_3$ must reflect spin-density wave ordering that originates in the Fermi surface nesting of the itinerant Kondo liquid.

Because for both materials the specific heat is enhanced by antiferromagnetic fluctuations only in a narrow range above T_N, we can safely neglect the relocalization correction; on doing so we obtain $S(T_N)$ of approximately 0.69 $R \ln 2$ for UPd$_2$Al$_3$ and 0.05 $R \ln 2$ for UNi$_2$Al$_3$, in good agreement with the experimental values of 0.67 $R \ln 2$ for UPd$_2$Al$_3$ and 0.12 $R \ln 2$ for UNi$_2$Al$_3$ (30). For UNi$_2$Al$_3$, we find $T_L = 39$ K and $\gamma_h = 75$ mJ/mol K^2, somewhat smaller than the experimental value of 150 mJ/mol K^2 (16).

YbAl$_3$. Our fit to the susceptibility of YbAl$_3$ (32) gives $f_0 = 1.5$, $\theta = 340$ K, and $T^* = 160$ K. This is consistent with the nonmagnetic ground state of this compound, for which we find $T_L = 38$ K. The specific heat coefficient is estimated to be $\gamma_h = 62$ mJ/mol K^2, consistent with the experimental value of 45 mJ/mol K^2.

For materials for which f_0 cannot be easily obtained, one can still estimate the entropy release by making the approximation $f_0 = 1$ in Eq. **11**. For antiferromagnetic compounds with $f_0 < 1$, a larger f_0 results in a smaller $S(T_N)$, which may cancel the effect of relocalization. Taking CePd$_2$Si$_2$ as an example, we predict $S(T_N) = 0.62 \, R \ln 2$ using $T_N = 9.9$ K and $T^* = 40$ K (4), quite close to the experimental value of $S(T_N) = 0.68 \, R \ln 2$ (42, 43). This suggests a rough relation between $S(T_o)$ and T_o/T^* ($T_o = T_c, T_N, T_L$, etc.) that can be easily applied to other materials in the future.

Conclusions

In summary, our introduction of hybridization effectiveness into the two-fluid description yields a viable alternative to the Doniach phase diagram (14) for heavy electrons, and its determination from experiment leads to a unified phenomenological explanation of heavy-electron magnetic properties. It will be important to extend the present analysis to a number of other heavy-electron materials and to determine the expected magnetic-field dependence of the hybridization-effectiveness parameter, f_0. An analysis of future experiments should yield a hybridization-based 3D pressure/magnetic-field phase diagram, tell us whether it is possible to place all heavy-electron materials on it, and establish the localization line for those materials with $f_0 > 1$. Experiments may also provide further information on the physical origin of f_0—e.g., does it scale with $J\rho$ and so mirror the Kondo coupling? At this stage, the improved two-fluid description presented here shows considerable promise as a candidate phenomenological standard model of heavy-electron emergent behaviors and should provide the basis for the development of a microscopic theory that explains these behaviors as a natural consequence of the coupling of the local-moment spin liquid to the conduction electron sea in which it is immersed.

1. Nakatsuji S, Pines D, Fisk Z (2004) Two fluid description of the Kondo lattice. *Phys Rev Lett* 92:016401.
2. Curro NJ, Young B-L, Schmalian J, Pines D (2004) Scaling in the emergent behavior of heavy-electron materials. *Phys Rev B Condens Matter Mater Phys* 70:235117.
3. Yang Y-F, Pines D (2008) Universal behavior in heavy-electron materials. *Phys Rev Lett* 100:096404.
4. Yang Y-F, Fisk Z, Lee H-O, Thompson JD, Pines D (2008) Scaling the Kondo lattice. *Nature* 454:611–613.
5. Yang Y-F, Urbano R, Curro NJ, Pines D, Bauer ED (2009) Magnetic excitations in the Kondo liquid: Superconductivity and hidden magnetic quantum critical fluctuations. *Phys Rev Lett* 103:197004.
6. Yang Y-F, Curro NJ, Fisk Z, Pines D, Thompson JD (2011) A predictive standard model for heavy electron systems. *J Phys Conf Ser* 273:012066.
7. apRoberts-Warren N, et al. (2011) Kondo liquid emergence and relocalization in the approach to antiferromagnetic ordering in CePt$_2$In$_7$. *Phys Rev B Condens Matter Mater Phys* 83:060408.
8. Shirer KR, et al. (2012) Long range order and two-fluid behavior in heavy electron materials. *Proc Natl Acad Sci USA* 45:3067–3073.
9. Mito T, et al. (2003) Coexistence of antiferromagnetism and superconductivity near the quantum criticality of the heavy-fermion compound CeRhIn$_5$. *Phys Rev Lett* 90:077004.
10. Kawasaki S, et al. (2003) Gapless magnetic and quasiparticle excitations due to the coexistence of antiferromagnetism and superconductivity in CeRhIn$_5$: A study of ^{115}In NQR under pressure. *Phys Rev Lett* 91:137001.
11. Park T, et al. (2006) Hidden magnetism and quantum criticality in the heavy fermion superconductor CeRhIn$_5$. *Nature* 440:65–68.
12. Kenzelmann M, et al. (2008) Coupled superconducting and magnetic order in CeCoIn$_5$. *Science* 321:1652–1654.
13. Bauer ED, et al. (2010) Pressure-induced superconducting state and effective mass enhancement near the antiferromagnetic quantum critical point of CePt$_2$In$_7$. *Phys Rev B Condens Matter Mater Phys* 81:180507.
14. Doniach S (1977) The Kondo lattice and weak antiferromagnetism. *Physica B Condens Matter* 91:231–234.
15. Hegger H, et al. (2000) Pressure-induced superconductivity in quasi-2D CeRhIn$_5$. *Phys Rev Lett* 84:4986–4989.
16. Curro NJ, et al. (2001) Anomalous NMR magnetic shifts in CeCoIn$_5$. *Phys Rev B Condens Matter Mater Phys* 64:180514.
17. Yokoyama M, Tenya K, Amitsuka A (2002) Thorium dilution effects of the heavy electron compound URu$_2$Si$_2$. *Physica B Condensed matter* 312–313:498–500.
18. Park T, et al. (2008) Isotropic quantum scattering and unconventional superconductivity. *Nature* 456:366–368.
19. Park T, Thompson JD (2009) Magnetism and superconductivity in strongly correlated CeRhIn$_5$. *New J Phys* 11:055062.
20. Kawasaki S, et al. (2002) Evolution of the magnetism and superconductivity in CeRhIn$_5$ under pressure: ^{115}In-NQR study. *J Phys Soc Jpn* 71:282–284.
21. Nakajima Y, et al. (2007) Non-Fermi liquid behavior in the magnetotransport of CeMIn$_5$ (M: Co and Rh): Striking similarity between quasi two-dimensional heavy fermion and high-T_c cuprates. *J Phys Soc Jpn* 76:024703.
22. Bao W, et al. (2002) Anisotropic three-dimensional magnetic fluctuations in heavy fermion CeRhIn$_5$. *Phys Rev B Condens Matter Mater Phys* 65:100505.
23. Aso N, et al. (2009) Switching of magnetic ordering in CeRhIn$_5$ under hydrostatic pressure. *J Phys Soc Jap* 78:073703.
24. Llobet A, et al. (2004) Magnetic structure of CeRhIn$_5$ as a function of pressure and temperature. *Phys Rev B Condens Matter Mater Phys* 69:024403.
25. Christianson AD, et al. (2002) Neutron scattering study of crystal fields in CeRhIn$_5$. *Phys Rev B Condens Matter Mater Phys* 66:193102.
26. Monthoux P, Pines D, Lonzarich GG (2007) Superconductivity without phonons. *Nature* 450:1177–1183.
27. Uemura YJ, et al. (1989) Universal correlations between T_c and n_s/m^* (carrier density over effective mass) in high-T_c cuprate superconductors. *Phys Rev Lett* 62:2317–2320.
28. Moriya T (1956) Nuclear magnetic relaxation in antiferromagnetics. *Prog Theor Phys* 16:23–44.
29. Curro NJ, et al. (2003) Low-frequency spin dynamics in the CeMIn$_5$ materials. *Phys Rev Lett* 90:227202.
30. Tateiwa N, Sato N, Komatsubara T (1998) Heat-capacity investigation on magnetism in UNi$_2$Al$_3$. *Phys Rev B Condens Matter Mater Phys* 58:11131–11133.
31. Mydosh JA, Oppeneer PM (2011) Hidden order, superconductivity, and magnetism: The unsolved case of URu$_2$Si$_2$. *Rev Mod Phys* 83:1301–1322.
32. Havinga EE, Buschow KHJ, van Daal HJ (1973) The ambivalence of Yb in YbAl$_2$ and YbAl$_3$. *Solid State Commun* 13:621–627.
33. De Visser A, et al. (1986) Specific heat, susceptibility and high-field magnetisation experiments on heavy fermion UPt$_3$ alloyed with Pd. *Phys Lett* 113:489–494.
34. Geibel C, et al. (1991) A new heavy-fermion superconductor: UNi$_2$Al$_3$. *Z Phys B Condensed Matter* 83:305–306.
35. Petrovic C, et al. (2001) Heavy-fermion superconductivity in CeCoIn$_5$ at 2.3 K. *J Phys Condens Matter* 13:L337–L342.
36. Sidorov VA, et al. (2002) Superconductivity and quantum criticality in CeCoIn$_5$. *Phys Rev Lett* 89:157004.
37. Bonn DA, Garrett JD, Timusk T (1988) Far-infrared properties of URu$_2$Si$_2$. *Phys Rev Lett* 61:1305–1308.
38. Aynajian P, et al. (2010) Visualizing the formation of the Kondo lattice and the hidden order in URu$_2$Si$_2$. *Proc Natl Acad Sci USA* 107:10383–10388.
39. Santander-Syro AF, et al. (2009) Fermi-surface instability at the "hidden-order" transition of URu$_2$Si$_2$. *Nat Phys* 5:637–641.
40. Dürkop D, et al. (1986) Antiferromagnetic order and 4f-instability of CePb$_3$. *Z Phys B Condens Matter* 63:55–61.
41. Grauel A, et al. (1992) Tetravalency and magnetic phase diagram in the heavy-fermion superconductor UPd$_2$Al$_3$. *Phys Rev B Condens Matter Mater Phys* 46:5818–5821.
42. Besnus MJ, Braghta A, Meyer A (1991) Kondo behavior in magnetic (Ce-La)Pd$_2$Si$_2$. *Z Phys B Condens Matter* 83:207–211.
43. Sheikin I, Wang Y, Bouquet F, Lejay P, Junod A (2002) Specific heat of heavy-fermion CePd$_2$Si$_2$ in high magnetic fields. *J Phys Condens Matter* 14:L543–L549.